International Journal of Fluid Mechanics Research, Vol. 29, No. 1, 2002

Numerical Modelling of Darcy – Brinkman – Forchheimer Magnetohydrodynamic Mixed Convection Flow in a Porous Medium with Transpiration and Viscous Heating[†]

A. J. Chamkha
Department of Mechanical Engineering,
Kuwait University, Safat, 13060 – Kuwait

H. S. Takhar
Department of Engineering, Manchester Metropolitan University,
Manchester, M15GD, UK

O. A. Beg
18 Milton Grove, Whalley Range,
Manchester, M16OBP, UK

A mathematical model is presented to investigate the combined effects of buoyancy, porous inertial drag, boundary vorticity diffusion (Brinkman friction), transverse magnetic field, viscous dissipation, wall transpiration, thermal conductivity and various other thermofluid parameters on the convection boundary layer flow of an electrically-conducting fluid past a vertical permeable semi-infinite plate in a saturated porous medium. The transformed boundary layer equations are solved numerically on a ξ-η domain using the robust Keller-box finite difference method and a powerful double-shooting Runge – Kutta method (DSRK). Results are presented graphically for the local skin-friction function (surface shear stress parameter) and the local Nusselt number function (local heat transfer parameter) for a wide range of the pertinent physical parameters. For the special case of $\xi = 0$ (at the leading edge), plots are given to compare the computations by both numerical methods and found to be in excellent agreement.

* * *

Nomenclature

f	dimensionless stream function;
u, v	velocities along x, y directions;
B	magnetic flux density;
g	acceleration due to gravity;

[†] Received 7.05.2000

ISSN 1064-2277

K	thermal conductivity;
C_p	specific heat at constant pressure;
T	temperature;
U_∞	free stream velocity (at edge of boundary layer);
T_w, T_∞	wall temperature, free stream temperature;
$\mathrm{Ec} = U_\infty^2/C_p\Delta T$	Eckert number;
$\mathrm{Gr} = \mathrm{g}\beta\Delta T L^3/\nu^2$	Grashof number;
$\mathrm{Pr} = \mu_f/\alpha_f\rho_f = \nu_f/\alpha_f$	Prandtl number;
$\mathrm{Da} = k/L^2$	Darcy number;
$\mathrm{Ha} = \left[\sigma B^2 L^2/\mu_f\right]^{1/2}$	Hartmann magnetic number;
$\mathrm{Re} = U_\infty L/\nu_f$	Reynolds number;
$\mathrm{Fs} = b/L$	Forchheimer number;
Nu	Nusselt number;
k	permeability of the porous medium;
b	Forchheimer constant;
L	standard reference length;
$V(x)$	suction velocity (negative for blowing).

Greek Symbols

$\alpha = U_\infty\delta\dot{\delta}/\nu_f$	boundary layer parameter;
α_m	thermal diffusivity;
β	coefficient of cubical expansion;
ε	porosity of the medium;
θ	dimensionless temperature variable;
σ	electrical conductivity;
$\nu_f = \mu_f/\rho_f$	fluid kinematic viscosity;
$\gamma = V\delta/\nu_f$	transpiration parameter;
κ	stagnant thermal conductivity of fluid-saturated porous medium;
κ_f	fluid thermal conductivity;
λ	thermal conductivity ratio;
μ_f	fluid dynamic viscosity;
μ'	effective viscosity of medium (Brinkman modified viscosity);
$\Lambda = \mu'/\mu_f$	fluid-matrix viscosity ratio;
$\delta = \left[2\alpha(x - x_0)\nu_f/U_\infty\right]^{1/2}$	boundary layer thickness;
η	spanwise pseudo-similarity coordinate;
ξ	streamwise pseudo-similarity coordinate;
ρ_f	fluid density;
ψ	stream function.

Superscripts

$'$	differentiation with respect to η;
$\cdot$	differentiation with respect to x.

Subscripts

f	fluid;
w	wall condition;
∞	free stream condition.

1. Introduction

Numerous studies have been performed in recent years to investigate the effects of various physical phenomena on boundary layer heat transfer in fluid-saturated porous media largely due to the extensive applications of this flow in metal casting technology, underground aquifer-energy storage, geothermal hydrology, ceramic soil mechanics, paper/textile insulation mechanisms in modern building structures [1]. Following the initial study of Cheng and Minkowycz [2] on Darcy convective flow in isotropic porous media many researchers analysed the effects of non-Darcian behavior, i. e., Forchheimer inertial resistance on flow and heat transfer in porous media. This study was precipitated by the realization of the inadequacy of Darcy's law in simulating higher-Reynolds number flows and capturing any realistic appraisal of boundary effects which are vitally important in for example geothermal heat transfer in the vicinity of rock strata and in materials processing. Vafai and Tien [3] were among the first researchers in boundary layer theory to study these so called non-Darcy effects in their analysis of boundary and inertial effects on forced convection along a flat plate in a porous medium; they used the Brinkman – Forchheimer – Extended Darcy (BFD) general flow model which basically incorporates a shearing stress term for boundary frictional resistance causing vorticity diffusion and a quadratic velocity term of porous inertia. A plethora of studies employing the BFD model have consequently been made. Lauriat and Prasad [4] investigated the effects of using the BFD model. Beckermann, et al. [5] numerically studied the Darcy – Forchheimer – Brinkman free convection in a vertical enclosure filled with a porous medium.

More recently other authors have examined the supplementary effects of magnetic field and viscous dissipation on convection in porous media.

Magnetohydrodynamic phenomena are invoked when fluids are electrically conducting as typified by geothermal salt-laden fluid subjected to the Earth's strong geomagnetic field. Many studies have been performed on magnetoconvective flows in porous media. Raptis and Kafousias [6] analysed the MHD free convective flow through a porous medium. Takhar and Ram [7] studied the effects of Hall currents on oscillatory MHD free convection in a porous medium. Takhar and Ram [8] also studied the MHD free convection flow of water at $4^{\circ}C$ through a porous medium. Takhar et al. [9] have also investigated the MHD convective flow of a heat generating fluid past a vertical plate in a porous medium with the supplementary effects of Hall currents and a constant heat flux. In practically all MHD analyses the Darcy model has been employed.

With respect to the important phenomenon of viscous dissipation, Gebhart [10] has highlighted the significance of viscous heating in geological flows which are generally of large-scale. Nakayama and Pop [11] recently examined the effects of viscous dissipation on the free convection flow over a non-isothermal body in porous medium. Takhar, Soundalgekar, and Gupta [12] examined the effects of non-Darcy behaviour and viscous heating in their recent study of Darcy-Brinkman mixed convection past a hot vertical plate in a porous medium. Very recently Takhar, Soundalgekar, and Beg [13] extended this study to include the effects of variable thermal conductivity in addition to higher magnitudes of viscous dissipation.

Buoyancy-induced convective flows constitute another widely-researched area of porous media convection having great applications in geothermal engineering, insulation systems, nuclear repository-modelling, and industrial drying/filtration systems. An early analysis was made by Cheng and Chang [14] who examined the convective flow induced by buoyancy forces adjacent to impermeable horizontal surfaces in a fully-saturated porous medium. Jang and Chang [15] have studied numerically the buoyancy-induced inclined boundary layer flow in a saturated porous medium. Poulikakos [16] has considered the buoyancy driven convective flow past a porous substrate. Nakayama and Koyama [17] obtained similarity solutions for the case of a buoyancy-induced

convection past a non-isothermal curved surface in a porous medium with the added feature of medium thermal stratification of the medium.

The effects of lateral mass flux, i. e., transpiration (suction/blowing) are also significant in geothermal recharging flows involving withdrawal and injection of hot fluids into reservoirs at boundaries. The important study of constant discharge velocity at uniform temperature in free convective boundary layer flow in a Darcian porous medium was performed by Merkin [18]. Other studies of transpiration effects on porous convection have been carried out by Huang and Chen [19], and Ramaniah and Malarvizhi [20].

The present study is aimed at collectively studying the combined effects of buoyancy parameter (Grashof number). Transpiration (lateral mass flux), Darcy bulk matrix resistance (Darcy effect), porous inertia (Forchheimer effect), boundary friction work and transverse magnetic field on the two dimensional thermal boundary layer flow in a porous medium past a vertical porous flat plate. The study may therefore be considered mathematical and numerical extension to the recent Darcy – Brinkman study by Takhar et al. [13] to include the effects of Forchheimer quadratic drag, transpiration, and magnetohydrodynamic body force. Such a study with the present mathematical model has not been performed thus far in the literature.

2. Theoretical Model and Mathematical Analysis

Under the classical Oberbeck – Boussinesq and Prandtl boundary layer approximations, the governing equations for magnetohydrodynamic heat and momentum transfer of an electrically-conducting fluid, e. g., salt-solution, past a hot vertical permeable plate in a non-Darcian porous medium with reference to a Cartesian coordinate x-y system may be stated as:

$$\frac{\partial u}{\partial x} + \frac{\partial v}{\partial y} = 0, \tag{1}$$

$$\frac{\rho_f}{\varepsilon^2}\left[u\frac{\partial u}{\partial x} + v\frac{\partial u}{\partial y}\right] = -\frac{\mu_f u}{k} + \rho_f \mathrm{g}\beta\left(T - T_\infty\right) + \frac{\mu'}{\varepsilon}\frac{\partial^2 u}{\partial y^2} - \frac{\rho_f b u^2}{k} - \sigma B^2 u, \tag{2}$$

$$\rho C_p\left[u\frac{\partial T}{\partial x} + v\frac{\partial T}{\partial y}\right] = K\frac{\partial^2 T}{\partial y^2} + \left(\frac{\partial u}{\partial y}\right)^2. \tag{3}$$

The physical scheme is depicted below in Fig. 1.

Here the x-axis is directed along the plate and the following important assumptions are made.

1. Thermophysical properties of the solid and the fluid are constant except for the buoyancy term.
2. Local thermal equilibrium is assumed between the solid matrix particles and the percolating fluid.
3. The magnetic field is applied transverse to the plate and assumed to be uniformly distributed.
4. The ratio of thermal diffusivity to magnetic difiusivity is small compared with unity and no magnetic induction is generated.
5. The porous medium is assumed to be two-dimensional, non-deformable, homogenous, and isotropic.
6. The effects of Joule heating, and hydrodynamic, and thermal dispersion are ignored.

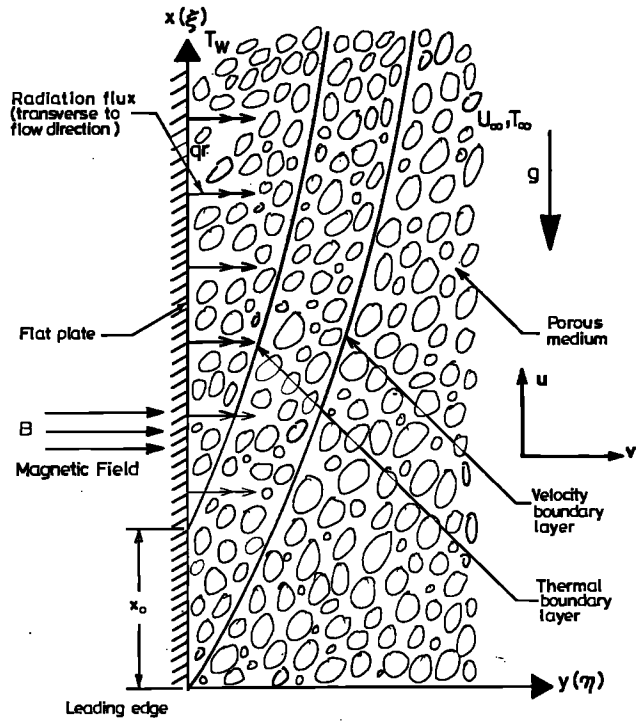

Fig. 1. Magnetohydrodynamic convection flow past a vertical porous plate.

7. The fluid is assumed viscous and incompressible.

The d'Alembert continuity equation (1) may be automatically satisfied with the introduction of a stream function ψ defined such that

$$u = \frac{\partial \psi}{\partial y}, \qquad v = -\frac{\partial \psi}{\partial x}. \tag{4}$$

We now implement the following pseudosimilarity transformations:

$$\begin{aligned} \psi &= U_\infty \delta(x) f(\xi,\eta) + \int v(x)dx, \qquad & \eta &= \frac{y}{\delta(x)}, \\ \xi &= \xi(x) = \frac{g\beta\,\Delta T \varepsilon^2 (x - x_0)}{U_\infty^2 L^2}, \qquad & \theta &= \frac{T - T_\infty}{T_w - T_\infty}. \end{aligned} \tag{5}$$

Clearly for the case of a solid plate, e. g., impermeable rock stratum, the transpiration parameter V is dropped in the stream-function definition, this being performed in an earlier study [13]. Substitution of transformations Eq. (5) into Eqs (1) – (3) culminates in the transformed dimensionless pseudo-similar boundary layer equations which take the form:

$$\begin{aligned} &f''' + f''(\alpha f + \gamma) + 2\alpha\xi \frac{\partial f}{\partial \xi}(f'') - 2\alpha\,\xi \frac{\partial^2 f}{\partial \xi \partial \eta}(f') + 2\alpha\xi(\theta) \\ &-2\alpha\xi \frac{\mathrm{Re}}{\mathrm{Gr\,Da}} f' - 2\alpha \frac{\mathrm{Fs\,Re}^2}{\mathrm{Da\,Gr}} f' - 2\alpha \frac{\mathrm{Fs\,Re}^2}{\mathrm{Da\,Gr}}(\xi) f'^2 = 0, \end{aligned} \tag{6}$$

$$\frac{\theta''}{\mathrm{Pr}} + \lambda\,\mathrm{Ec}\,(f'')^2 + \lambda\,(\alpha f + \gamma)\,\theta' + 2\,\alpha\,\lambda\,\xi\,\theta'\,\frac{\partial f}{\partial \xi} - 2\,\alpha\,\lambda\,\xi\,f'\,\frac{\partial \theta}{\partial \xi} = 0. \tag{7}$$

The appropriate boundary conditions are:

$$\begin{aligned} &\eta = 0: \quad f(\xi) = 0, \quad f'(\xi) = 0, \quad \theta(\xi) = 1; \\ &\eta \to \infty: \quad f'(\xi) = 1, \quad \theta(\xi) = 0. \end{aligned} \tag{8}$$

3. Computational Solution by Implicit Keller-Box Method

The pseudo-similarity equations (6) and (7) together with boundary conditions Eq. (8) are to be solved with the implicit central finite-differencing Keller-Box scheme employing Newton quazi-linearization and block tridiagonal elimination described at length by Cebeci and Bradshaw [21]. The boundary layer similarity equations, are reduced to a set of five first order ordinary differential equations by introducing new unknown functions of η-derivatives:

$$f' = U, \qquad U' = V, \qquad \theta' = G,$$

$$\begin{aligned} &V' + \alpha f V + \gamma V - 2\alpha\,\frac{\mathrm{Fs}\,\mathrm{Re}^2}{\mathrm{Da}\,\mathrm{Gr}}\xi U^2 - 2\alpha\,\frac{\mathrm{Re}\,\mathrm{Ha}^2}{\mathrm{Gr}}\xi U + 2\alpha\xi\theta \\ &\quad -2\alpha\,\frac{\mathrm{Re}}{\mathrm{Gr}\,\mathrm{Da}}\xi U - 2\alpha\left(U\frac{\partial U}{\partial \xi} - V\frac{\partial f}{\partial \xi}\right) = 0, \\ &\frac{G'}{\mathrm{Pr}} + \lambda \mathrm{Ec} V^2 + \lambda\alpha f G + \lambda\gamma G - 2\alpha\xi\lambda\left(U\frac{\partial \theta}{\partial \xi} - G\,\frac{\partial f}{\partial \xi}\right) = 0 \end{aligned} \tag{9}$$

and the boundary conditions become:

$$\begin{aligned} &f(\xi, 0) = 0, \quad U(\xi, 0) = 0, \quad \theta(\xi, 0) = 1; \\ &U(\xi, \infty) = 1, \quad \theta(\xi, \infty) = 0. \end{aligned} \tag{10}$$

A 2-dimensional finite-difference mesh is now superimposed on the ξ-η plane defined by:

$$\begin{aligned} &\xi_0 = 0, \quad \xi_n = \xi_{n-1} + k_n, \quad n = 1, \ldots, N; \\ &\eta_0 = 0, \quad \eta_j = \eta_{j-1} + h_j, \quad j = 1, \ldots, J. \end{aligned} \tag{11}$$

If Z designates the value of any variable at (ξ^n, η_j), then the functions and derivatives of Eqs (9) at $(\xi^{n-1/2}, \eta_{j-1/2})$ are replaced by the expressions:

$$\begin{aligned} Z_{j-1/2}^{n-1/2} &= \frac{Z_j^n + Z_{j-1}^n + Z_j^{n-1} - Z_{j-1}^{n-1}}{4}, \\ \left(\frac{\partial Z}{\partial \xi}\right)_{j-1/2}^{n-1/2} &= \frac{Z_j^n + Z_{j-1}^n - Z_j^{n-1} - Z_{j-1}^{n-1}}{4k_n}, \\ \left(\frac{\partial Z}{\partial \eta}\right)_{j-1/2}^{n-1/2} &= \frac{Z_j^n + Z_{j-1}^n - Z_j^{n-1} - Z_{j-1}^{n-1}}{4h_j}. \end{aligned} \tag{12}$$

Approximating the quantities f, U, V, θ, G at the points ξ^n, η_j on the net by f_j^n, U_j^n, V_j^n, θ_j^n, G_j^n generates the following set of non-linear algebraic equations:

$$h_j^{-1}\left(f_j^n - f_{j-1}^n\right) = U_{j-1/2}^n, \tag{13a}$$

$$h_j^{-1}\left(U_j^n - U_{j-1}^n\right) = V_{j-1/2}^n, \tag{13b}$$

$$h_j^{-1}\left(\theta_j^n - \theta_{j-1}^n\right) = G_{j-1/2}^n, \tag{13c}$$

$$\begin{aligned} &h_j\left(V_j^n - V_{j-1}^n\right) + K_1\left(f\,V\right)_{j-1/2}^n + K_2\,V_{j-1/2}^n + K_5\,\xi^{n-1/2}\,U_{j-1/2}^n \\ &-K_6\,\xi^{n-1/2}\,U_{j-1/2}^n - K_7\,\xi^{n-1/2}\left(U^2\right)_{j-1/2}^n + K_4\,\xi^{n-1/2}\,\theta_{j-1/2}^n \\ &- K_3\left(\xi^{n-1/2}/k_n\right)\left[\left(U^2\right)_{j-1/2}^n - \left(V_{j-1/2}^n\,f_{j-1/2}^n - V_{j-1/2}^n\,f_{j-1/2}^{n-1}\right.\right. \\ &\left.\left. + V_{j-1/2}^{n-1}\,f_{j-1/2}^n\right)\right] = R_{j-1/2}^{n-1}, \end{aligned} \tag{13d}$$

$$\begin{aligned} &h_j^{-1}\left(e_j^n\,G_j^n - e_{j-1}^n\,G_{j-1}^n\right) + K_1\left(f\,G\right)_{j-1/2}^n + K_2\,G_{j-1/2}^n + K_9\left(V^2\right)_{j-1/2}^n \\ &- K_3\left(\xi^{n-1/2}/k_n\right)\left[\left(U\,\theta\right)_{j-1}^n - U_{j-1/2}^n\,\theta_{j-1/2}^{n-1} + U_{j-1/2}^{n-1}\,\theta_{j-1/2}^n - \left(f\,G\right)_{j-1/2}^n\right. \\ &\left. - G_{j-1/2}^n\,f_{j-1/2}^{n-1} + G_{j-1/2}^{n-1}\,f_{j-1/2}^n\right] = T_{j-1/2}^{n-1}, \end{aligned} \tag{13e}$$

where h_j denote the η-step distance and k_n designates the ξ-step length and where the coefficients K_1 to K_9 are defined as follows:

$$\begin{aligned} &K_1 = \alpha, \quad K_3 = K_4 = 2\,\alpha, && K_6 = 2\,\alpha\left(\mathrm{Re}/\mathrm{Gr}\,\mathrm{Da}\right), && K_8 = 1/\lambda\,\mathrm{Pr}, \\ &K_2 = \gamma, \quad K_5 = 2\alpha\left(\mathrm{Ha}^2\,\mathrm{Re}/\mathrm{Gr}\right), && K_7 = 2\alpha\left(\mathrm{Fs}\,\mathrm{Re}^2/\mathrm{Da}\,\mathrm{Gr}\right), && K_9 = \mathrm{Ec}. \end{aligned} \tag{14}$$

The residual functions $R_{j-1/2}^{n-1}$ and $T_{j-1/2}^{n-1}$ are given by:

$$\begin{aligned} R_{j-1/2}^{n-1} &= h_j^{-1}\left(V_j^{n-1} - V_{j-1}^{n-1}\right) - K_1\left(fV\right)_{j-1/2}^{n-1} - K_2 V_{j-1/2}^{n-1} + K_5\,\xi^{n-1/2} U_{j-1/2}^{n-1} \\ &+K_6\xi^{n-1/2} U_{j-1/2}^{n-1} + K_7\xi^{n-1/2}\left(U^2\right)_{j-1/2}^{n-1} - K_4\xi^{n-1/2}\theta_{j-1/2}^{n-1} - K_3\left(\xi^{n-1/2}/k_n\right) \\ &\times\left(U^2\right)_{j-1/2}^{n-1} V_{j-1/2}^{n-1} f_{j-1/2}^{n-1}, \end{aligned} \tag{15}$$

$$\begin{aligned} T_{j-1/2}^{n-1} &= -h_j^{-1}\left(e_j^{n-1} G_j^{n-1} - e_{j-1}^{n-1} G_{j-1}^{n-1}\right) - K_1\left(fG\right)_{j-1/2}^{n-1} - K_2 G_{j-1/2}^{n-1} \\ &-K_9\left(V^2\right)_{j-1/2}^{n-1} + K_3\left(\xi^{n-1/2}/k_n\right)\left[\left(fG\right)_{j-1/2}^{n-1} - \left(U\theta\right)_{j-1/2}^{n-1}\right]. \end{aligned} \tag{16}$$

The equations (13a)–(13e) are solved using Newton's quasilinearisation technique followed by a block-factorization technique discussed by Keller [22, 23]. This technique has been applied very effectively by many investigators including Cebeci and Smith [24], Ingham and Pop [25], Hossain [26], and Gorla and Pop [27]. The initial profiles for functions f, U, V, θ, G are generated using a subroutine IVPL, and then used to march along the boundary layer in the streamwise direction solving for ξ. The surface shear stress, i. e., local skin friction function $C_f/(2\mathrm{Re}_x^{-1/2})$ and local heat transfer parameter, i. e., local Nusselt number function are $\mathrm{Nu}_x/\mathrm{Re}_x^{1/2}$ defined in terms of the wall boundary layer functions $V(\xi,0)$ and $G(\xi,0)$ according to:

$$C_f/\mathrm{Re}_x^{-1/2} = V\left(\xi,0\right), \qquad -\mathrm{Nu}_x/\mathrm{Re}_x^{1/2} = G\left(\xi,0\right). \tag{17}$$

4. Double Shooting Runge – Kutta – Merson (DSRKM) Solutions

We now derive solutions for the pseudo-similarity equations (6) and (7) using the numerical equivalent of the method of matched asymptotic expansions, viz., the series expansion technique followed by numerical integration using double shooting Runge – Kutta – Merson quadrature. Details of computational aspects are available in the recent study by Gorla and Takhar [28]. Taylor expansions are carried out for f and θ valid for $\xi < 1$ as follows:

$$\begin{aligned} f(\xi,\eta) &= f_0(\eta) + \xi\, f_1(\eta) + \xi^2\, f_2(\eta) + \xi^3\, f_3(\eta) + \xi^4\, f_4(\eta) + \ldots, \\ \theta(\xi,\eta) &= \theta_0(\eta) + \xi\, \theta_1(\eta) + \xi^2\, \theta_2(\eta) + \xi^3\, \theta_3(\eta) + \xi^4\, \theta_4(\eta) + \ldots \end{aligned} \tag{18}$$

Truncating expansions at fourth order and abbreviating $\mathrm{Ha}^2\,\mathrm{Re}/\mathrm{Gr}$, $\mathrm{Fs}\,\mathrm{Re}^2/(\mathrm{Da}\,\mathrm{Gr})$ and $\mathrm{Re}/(\mathrm{Gr}\,\mathrm{Da})$ as Π_1, Π_2, Π_3 respectively, subsequent substitution of the expansions and their derivatives in the momentum and temperature equations produces a set of ten ordinary differential equations for the boundary layer flow, viz.:

$$f_0''' + (\alpha\, f_0 + \gamma) f_0'' = 0, \tag{19a}$$

$$f_1''' + (\alpha f_0 + \gamma) f_1'' + 3\alpha f_0'' f_1 - 2\alpha f_0'' f_1' + 2\alpha\theta_0 - 2\alpha\Pi_1 f_0' - 2\alpha\Pi_3 f_0' - 2\alpha\Pi_2 f'^2_0 = 0, \tag{19b}$$

$$\begin{aligned} &f_2''' + 5\alpha f_2 f_0'' + 3\alpha f_1'' f_1 + (\alpha f_0 + \gamma) f_2'' - 4\alpha f_0' f_2' - 2\alpha f_1' f_1' + 2\alpha\theta_1 \\ &-2\alpha\Pi_3 f_1' - 2\alpha\Pi_2 f_1' - 4\alpha\Pi_2 f_1' f_0' = 0, \end{aligned} \tag{19c}$$

$$\begin{aligned} &f_3''' + (\alpha f_0 + \gamma) f_3'' + 3\alpha f_1 f_2'' + 7\alpha f_0'' f_3 + 5\alpha f_1'' f_2 - 6\alpha f_0' f_3' - 6\alpha f_1' f_2' \\ &+2\alpha\theta_2 - 2\alpha\Pi_3 f_2' - 2\alpha\Pi_1 f_2' - 2\alpha\Pi_2 (2 f_0' f_2' + (f_1')^2) = 0, \end{aligned} \tag{19d}$$

$$\begin{aligned} &f_4''' + f_4''(\alpha f_0 + \gamma) + 3\alpha f_1 f_3'' + 7\alpha f_1'' f_3 + 5\alpha f_2'' f_2 + 9\alpha f_0'' f_4 - 2\alpha(4 f_0' f_4' \\ &+4 f_1' f_3' + 2(f_2')^2) + 2\alpha\theta_3 - 2\alpha\Pi_3 f_3' - 2\alpha\Pi_1 f_3' - 2\alpha\Pi_2 (2 f_0' f_3' + 2 f_1' f_2') = 0, \end{aligned} \tag{19e}$$

$$\theta_0'' + \mathrm{Pr}\lambda(\alpha f_0 + \gamma)\theta_0' + \mathrm{Pr}\lambda\mathrm{Ec}(f_0'')^2 = 0, \tag{19f}$$

$$\theta_1'' + 2\mathrm{Pr}\lambda\mathrm{Ec} f_0'' f_1'' + 2\alpha\mathrm{Pr}\lambda f_1\theta_0' + \mathrm{Pr}\lambda[(\alpha f_0 + \gamma)\theta_1' + \alpha f_1\theta_0'] - 2\alpha\mathrm{Pr}\lambda f_0'\theta_1 = 0, \tag{19g}$$

$$\begin{aligned} &\theta_2'' + \mathrm{Pr}\lambda\mathrm{Ec}[2 f_0'' f_2'' + (f_1'')^2] + \mathrm{Pr}\lambda(\alpha f_0 + \gamma)\theta_2' + \mathrm{Pr}\lambda\alpha(f_1\theta_1' + f_2\theta_0') \\ &+2\alpha\mathrm{Pr}\lambda(2\theta_0' f_2 + \theta_1' f_1) - 2\alpha\mathrm{Pr}\lambda(2 f_0'\theta_2 + f_1'\theta_1) = 0, \end{aligned} \tag{19h}$$

$$\begin{aligned} &\theta_3'' + 2\mathrm{Pr}\lambda\mathrm{Ec}(f_1'' f_2'' + f_0'' f_3'') + \mathrm{Pr}\lambda[(\alpha f_0 + \gamma)\theta_3' + \alpha f_1\theta_2' + \alpha f_2\theta_1' + \alpha f_3\theta_0'] \\ &+2\alpha\mathrm{Pr}\lambda(3\theta_0' f_3 + 2\theta_1' f_2 + f_1\theta_2') - 2\alpha\mathrm{Pr}\lambda(3 f_0'\theta_3 + 2 f_1'\theta_2 + f_2'\theta_1) = 0, \end{aligned} \tag{19i}$$

$$\begin{aligned} &\theta_4'' + \mathrm{Pr}\lambda\mathrm{Ec}[2 f_1'' f_3'' + 2 f_0'' f_4'' + (f_2'')^2] + \mathrm{Pr}\lambda[(\alpha f_0 + \gamma)\theta_4' + \alpha f_1\theta_3' + \alpha f_2\theta_2' \\ &+\alpha f_3\theta_1' + \alpha f_4\theta_0'] + 2\alpha\mathrm{Pr}\lambda(4 f_4\theta_0' + 3\theta_1' f_3 + 2\theta_2' f_2 + \theta_3' f_1) - 2\alpha\mathrm{Pr}\lambda(4 f_0'\theta_4 \\ &+3 f_1'\theta_3 + 2 f_2'\theta_2 + f_3'\theta_1) = 0. \end{aligned} \tag{19j}$$

The NAG library subroutine D02HBF is used to perform the numerical integration of these highly non-linear equations, which are broken down into 25 first order differential equations in terms of new functions F_i and their derivatives y_i. D02HBD contains approximately 30 auxiliary

subroutines such as FCN, D02HAW, D02HBR, D02SAX, F02WAY, X04ABF, etc., the respective subroutines performing various tasks. For example, FCN evaluates the derivatives y_i, F02SZF performs linear algebraic computations, X04AAF registers explanatory error messages. The number of unknown parameters N_1 (boundary values) must not exceed the number of differential equations. If $N_1 < N$, then $(N - N_1)$ equations of the system are not invoked in the "marching" process and the integration process is controlled by these "driving equations" are always specified first in the program. The boundary conditions are specified where possible and initially guesses are made of f'' and θ' for all orders since these are not known at the start of the computation. The subroutine calls up a Newton iterative solver which rectifies the values of the guesses boundary conditions until the forward and backward integration profiles (hence, "double shooting") match exactly to within a pre-set convergence criterion. This iteration routine solution, y_i, with respect to the j-th boundary condition parameter, denoted $P(J)$. The matrix is calculated by a basic numerical differentiation technique which requires N_1 integrations of the multiple first order differential system, where N_1 designates the number of unknown boundary conditions (parameters). Runge – Kutta – Merson quadrature is used in the integration process. Generally, the best direction of integration is that of decreasing solutions and is controlled by D02BAF. The state of the iterations is monitored progressively and convergence is usually attained within minutes. Numerical stability is very sensitive to the size of the η-step and a value around 0.1 or 0.2 generally ensures robust programming.

The boundary conditions are specified as follows:

$$
\begin{aligned}
& f_0(0) = f_0'(0) = f_1(0) = f_1'(0) = f_2(0) = f_2'(0) = 0, \\
& f_3(0) = f_3'(0) = f_4(0) = f_4'(0) = 0, \\
& \theta_0(0) = 1, \quad \theta_1(0) = \theta_2(0) = \theta_3(0) = \theta_4(0) = 0, \\
& f_0'(\infty) = f_1'(\infty) = f_2'(\infty) = f_3'(\infty) = f_4'(\infty) = 0, \\
& \theta_0(\infty) = 1, \quad \theta_1(\infty) = \theta_2(\infty) = \theta_3(\infty) = \theta_4(\infty) = 0.
\end{aligned}
\tag{20}
$$

5. Results and Discussion

In this section, numerical results for the surface shear stress $V(\xi, 0)$, i. e., local skin friction function and local heat transfer $G(\xi, 0)$, i. e., local Nusselt number function profiles computed with the Keller-Box method, versus streamwise variable for various Ec, Ha, Gr, Pr, Da, Fs, Re, γ, and λ are reported. In addition, graphs depicting the hierarchy of velocity functions f_o', f_1', f_2', f_3', f_4', and temperature functions θ_0, θ_1, θ_2, θ_3, θ_4, with spanwise coordinate η generated with DSRK technique are presented for a number of values of Ec, Ha, Gr, Pr, Da, Fs, γ, and λ. A representative set of graphical results is presented in Figs 2 through 14.

The effects of various transpiration parameter values γ on local skin friction function (surface shear stress $f''(\xi, 0)$) and local Nusselt number function (local heat transfer $\theta'(\xi, 0)$) are given in Figs 2a, b. Gebhart et al. [29] have indicated that the effects of lateral mass flux, i. e., suction/blowing can arise in geothermal systems with the lateral flow directed into or not of the vertical surface. Positive γ (suction) corresponds to material removal from the boundary layer and enhances $V(\xi, 0)$. The opposite effect is caused by negative γ (blowing) which implies mass injection into the boundary layer and a concomitant decrease in surface (local) shear stress. The magnitude of $G(\xi, 0)$ is reduced with blowing ($\gamma = -0.5, -1.0$) and increased with suction ($\gamma = 0.5, 1.0$).

The effects of the viscous dissipation parameter – Eckert number Ec – are depicted in Fig. 3.

As Ec rises from 0, corresponding to zero viscous dissipation to moderately high positive values of 0.2 and 0.4, local skin friction $C_f/(2\mathrm{Re}_x^{1/2})$ or $V'(\xi,0)$ is clearly enhanced. The converse behavior is apparent for negative Ec values which cause a reduction in $V(\xi,0)$ since velocities are now increased as the plate is heated. Local Nusselt number function magnitude $\mathrm{Nu}_x/\mathrm{Re}_x^{1/2}$ or $G(\xi,0)$ is markedly increased by negative Ec values and lowered for positive Ec values associated with cooling of the plate.

From other results not presented herein for brevity, the effects of the buoyancy parameter Gr on local skin friction function $V(\xi,0)$ and local Nusselt number function $G(\xi,0)$ were observed. Both $V(\xi,0)$ and $G(\xi,0)$ increased in magnitude as Gr was increased from 10 to 250, the latter corresponding to very strong buoyancy forces as encountered in hyper-active reservoirs. In addition, the local skin friction $V(\xi,0)$ and local Nusselt Number function $G(\xi,0)$ profiles versus ξ for various values of the magnetic parameter Ha, described in detail by Chandrasekhar [30] were obtained. A fall in $V(\xi,0)$, i. e., local shear stress parameter was observed with rising Hartmann number Ha due to the opposing nature of the magnetohydrodynamic effect, this acting as an extra body force term. A large decrease in local heat transfer parameter $G(\xi,0)$ also occurred as Ha raised from 0 which implies purely hydrodynamic flow (no electrical conduction) to $\mathrm{Ha}=8.0$ (strong magnetic field). Increasing the magnetic field strength generates increased interaction between the fluid motion and the transverse field causing an elevation in the magnitude of the Lorentz body force. This force due to its opposition to buoyancy produces a decrease in fluid velocities, and manifests as a depression in the local heat transfer and therefore intuitively also in the local Nusselt number function $\mathrm{Nu}_x/\mathrm{Re}_x^{1/2}$.

Porous resistance effects embodied in the Darcy and Forchheimer terms and numbers Da and Fs were also obtained. Since $\mathrm{Fs}=0.55Da^{1/2}$, the number Fs increases faster than Da for higher Da values (larger permeablility). Elevation in Da from 0.002 ($\mathrm{Fs}=0.02458$) to $\mathrm{Da}=0.05$ ($\mathrm{Fs}=0.12298$) induced a large increase in the surface shear stress, since although rising Da implies greater matrix permeability ($\mathrm{Da}\to\infty$ corresponds to the pure fluid regime, i. e., no porous matrix) and therefore less bulk matrix resistance the corresponding increase in Fs had a smaller influence, i. e., second order drag which is directly proportional to Fs and $(f')^2$ for a given Re, Gr, Da, α reduced velocities to a lesser extent producing an enhancement in local skin friction function $V(\xi,0)$. An increase in local heat transfer, i. e., Nusselt number function $\mathrm{Nu}_x/(2\mathrm{Re}_x^{1/2})$ or $G(\xi,0)$ magnitudes was apparent over the small range of increasing Da and Fs. This is explained by the fact that rising Da physically means higher permeability, less bulk matrix resistance, reduction in conduction by solid matrix particles and an increase in the diffusion of thermal energy by convection heat transfer due to the increased thermal activity, as indicated by Lauriat and Prasad [4].

The effects of various thermal conductivity ratios λ on local skin friction function $V(\xi,0)$ (i. e., surface shear stress $f''(\xi,0)$) and local Nusselt number function $\mathrm{Nu}_x/\mathrm{Re}_x^{1/2}$ (local heat transfer $\theta'(\xi,0)$) are provided in Figs 4a, b. As λ is increased from 0.5 to 2.5, a distinct reduction in the local skin friction occurs. An increase in the local Nusselt number function magnitude accompanies a rise in λ from 0.5 to 2.5.

The effects of Prandtl number Pr on local skin friction function, i. e., surface shear stress $V(\xi,0)$ and local Nusselt number function $\mathrm{Nu}_x/\mathrm{Re}_x^{1/2}$ or local heat transfer $\theta'(\xi,0)$ are given in Figs 5a, b. Values of Pr have been selected to represent a wide variety of engineering and hydrological fluids. $\mathrm{Pr}=0.02$ corresponds to the lower range for geophysical liquid metals and nuclear reactor fluids; Pr of 4.35 is taken to represent a realistic value for low temperature aquifers, e. g., geothermal water at 40°C. Rising Pr causes a large fall in the local skin friction (shear stress) accompanied by rising velocities. Prasad and Kladias [31] have shown that velocities increase substantially with Pr for $\mathrm{Pr}<10$, (provided Darcy and Grashof numbers have moderate values) which

is the range of interest in the present study. On the other hand, a substantial increase in local Nusselt number magnitude occurs as Pr rises from 0.02 through 0.733 (air), 1.0 (geothermal water) to 2.22 and 4.34 (low temperature hydrolgoical aquifers).

Local skin friction $V(\xi, 0)$ and Nusselt number function $G(\xi, 0)$ profiles versus ξ, for various Reynolds numbers Re are shown in Figs 6a, b. As Re is increased from 1.0 through 10.0 (limit for the Darcy law) up to 50.0, a dramatic fall in $V(\xi, 0)$ occurs since velocities increase with Re. Similarly $G(\xi, 0)$ magnitudes are substantially reduced as Re rises from 1 to 50.

Figs 7a, b to Figs 10a, b show the variation of the velocity and temperature field functions f_1', f_2', f_3', f_4', and θ_1, θ_2, θ_3, θ_4, with the spanwise coordinate η for various Grashof numbers obtained with the double shooting Runge – Kutta – Merson Method (DSRK). As Gr is raised from 100 to 300 (very strong buoyancy forces) velocities f_1' (Fig. 7a) and f_2' (Fig. 8b) both decrease, while f_3' (Fig. 9a), f_4' (Fig. 10a) both increase in magnitude respectively.

Temperature functions θ_1 (Fig. 7b), θ_2 (Fig. 8b), and θ_4 (Fig. 10b) all increase in magnitude while θ_3 (Fig. 9b) decreases as Gr rises from 100 to 300.

Figs 11a, b to Figs 14a, b show the variation of the velocity f_o', f_1', f_2', f_3', f_4', and temperatures θ_0, θ_1, θ_2, θ_3, θ_4, with η for various transpiration parameters γ. As γ increases form 0.0 to 2.0, an increase in velocities occurs; the converse is apparent for negative γ of -1.0 associated with blowing. On the other hand, temperatures decreases with rising γ (1.0, 2.0) with corresponds to suction, and increase dramatically for negative γ of -1.0 (blowing). In both cases, the Keller and DSRK profiles are exactly superimposed demonstrating excellent agreement between these two numerical schemes. The velocity functions f_1' (Fig. 11a), f_2' (Fig. 12a), f_3' (Fig. 13a), f_4' (Fig. 14a) all decrease in magnitude as γ is increased to 2.0 (suction). Temperatures θ_1 (Fig. 11b), θ_2 (Fig. 12b), θ_3 (Fig. 13b), θ_4 (Fig. 14b) also all decrease in magnitude as γ is raised from 0.0 (no transpiration) to 2.0 (suction).

6. Concluding Remarks

A laminar boundary layer analysis of magnetoconvection heat transfer in a non-Darcian porous medium with variable physical properties has been performed. From the numerical solutions to the pseudosimilar boundary layer equations we can conclude the following.

1. Generally, local skin friction function $V(\xi, 0)$ is increased in magnitude by rising Grashof number, suction ($\gamma > 0$), positive Ec, and Darcy and Forchheimer numbers; conversely rising Ha, λ, Pr, Re, and negative γ (blowing), and Ec all reduce local shear stresses.

2. Local Nusselt number function is increased in magnitude by increasing Gr, positive γ, negative Ec, rising Da, Fs, λ, Pr, and depressed by increasing negative γ, Ha, positive Ec, and Re.

3. Magnitude of the fluid velocity f_0 rises with positive γ and f_1', f_2', f_3', f_4' magnitudes generally fall with rising γ (suction); f_1', f_2' decrease with rising Gr; f_3', f_4' increase with rising Gr.

4. Temperature θ_0, falls with rising positive γ (suction); temperature θ_1, θ_2, θ_3, θ_4 generally increase with rising Gr and fall with rising suction.

Both Keller's method and the shooting scheme seem to produce excellent results and are presently being employed by the authors to extend the current to examine the effects of Joule magnetic heating, thermal stratification, and viscoelastic fluid behavior in porous continuum convection flows.

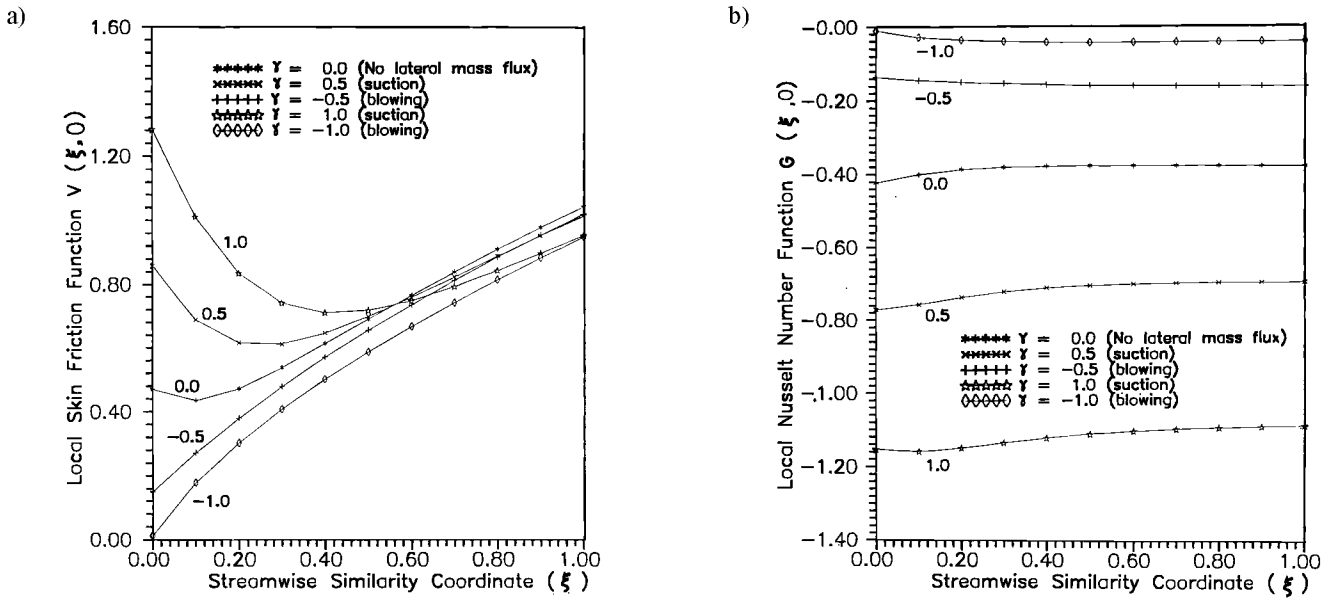

Fig. 2. Variation of $V(\xi, 0)$, i. e., $f''(\xi, 0)$, and $G(\xi, 0)$, i. e., $\theta'(\xi, 0)$ with streamwise coordinate ξ at the plate surface ($\eta = 0$) for various transpiration parameters (γ); results for Keller Box: $\alpha = 1.0$, $\mathrm{Gr} = 100$, $\mathrm{Da} = 0.01$, $\mathrm{Ha} = 1.0$, $\mathrm{Re} = 1.0$, $\mathrm{Pr} = 1.0$, $\mathrm{Ec} = 0.2$, $\lambda = 1.0$, $\mathrm{Fs} = 0.055$.

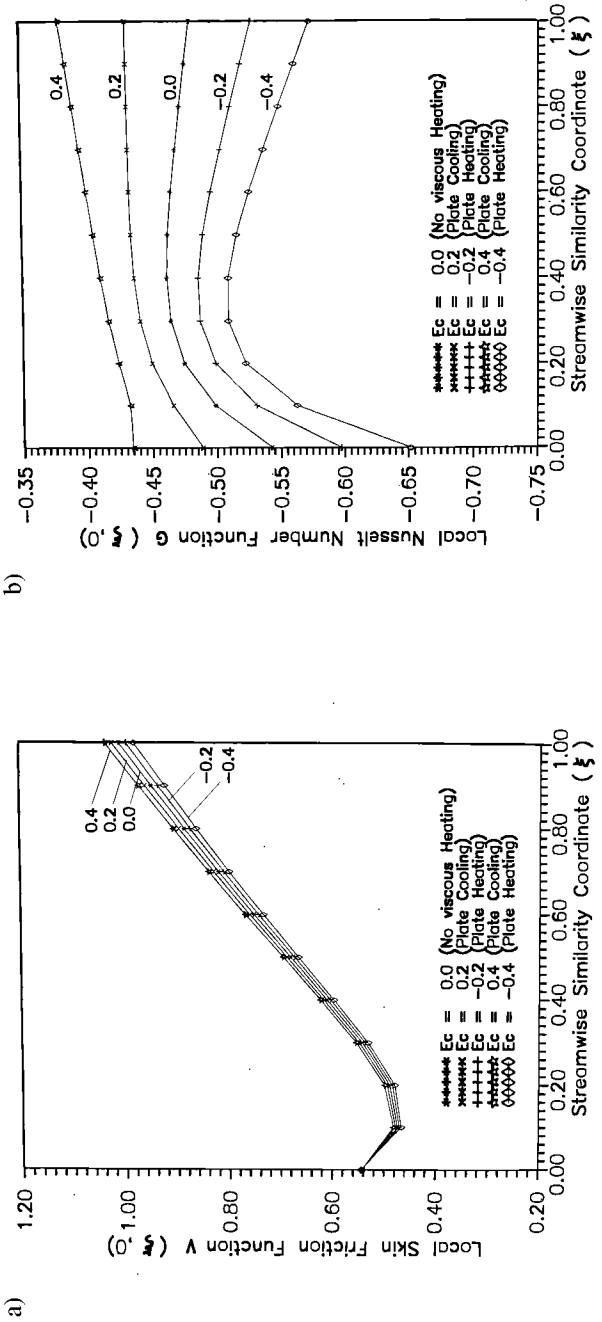

Fig. 3. Variation of $V(\xi, 0)$ and $G(\xi, 0)$ with streamwise coordinate ξ at the plate surface ($\eta = 0$) for various Eckert numbers (Ec); results for Keller Box: $\alpha = 1.0$, $\gamma = 0.1$, $\mathrm{Gr} = 100$, $\mathrm{Da} = 0.01$, $\mathrm{Re} = 1.0$, $\mathrm{Pr} = 1.0$, $\mathrm{Ha} = 1.0$, $\lambda = 1.0$, $\mathrm{Fs} = 0.055$.

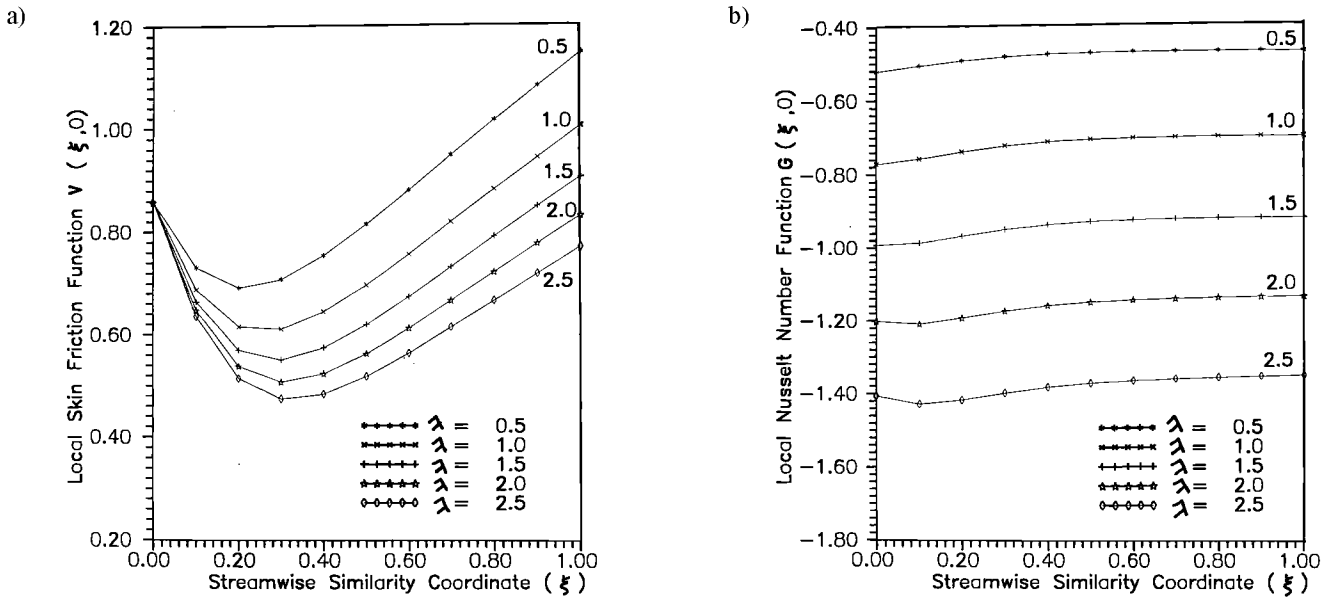

Fig. 4. Variation of $V(\xi, 0)$ and $G(\xi, 0)$ with streamwise coordinate ξ at the plate surface ($\eta = 0$) for various thermal conductivity ratios (λ); results for Keller Box : $\alpha = 1.0$, $\mathrm{Gr} = 100$, $\mathrm{Da} = 0.01$, $\mathrm{Re} = 1.0$, $\mathrm{Ha} = 1.0$, $\mathrm{Ec} = 0.2$, $\gamma = 0.5$, $\mathrm{Fs} = 0.055$, $\mathrm{Pr} = 1.0$ (geothermal water).

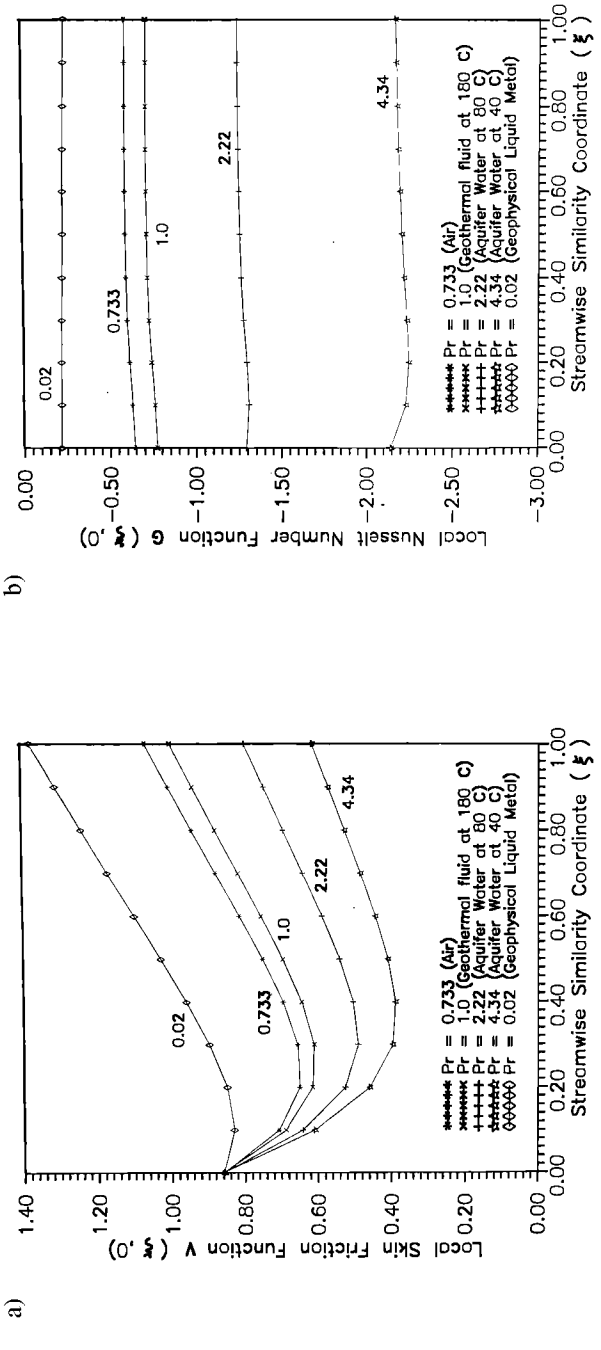

Fig. 5. Variation of $V(\xi,0)$ and $G(\xi,0)$ with streamwise coordinate ξ at the plate surface ($\eta = 0$) for various Prandtl numbers (Pr); results for Keller Box : $\alpha = 1.0$, $\gamma = 0.5$, $\mathrm{Gr} = 100$, $\mathrm{Da} = 0.01$, $\mathrm{Re} = 1.0$, $\mathrm{Ha} = 1.0$, $\mathrm{Ec} = 0.2$, $\lambda = 1.0$, $\mathrm{Fs} = 0.055$.

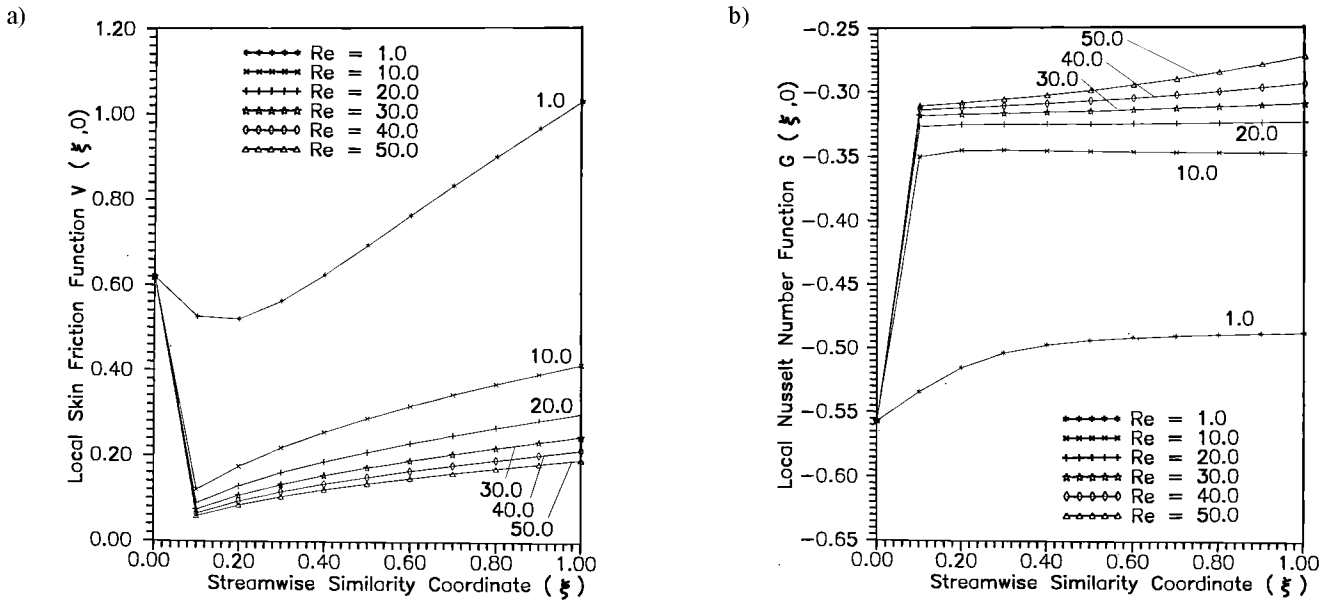

Fig. 6. Variation of $V(\xi, 0)$ and $G(\xi, 0)$ with streamwise coordinate ξ at the plate surface ($\eta = 0$) for various Reynolds numbers (Re); results for Keller Box : $\alpha = 1.0$, $\gamma = 0.2$ (suction), $\mathrm{Gr} = 100$, $\mathrm{Da} = 0.01$, $\mathrm{Re} = 1.0$, $\mathrm{Ha} = 1.0$, $\mathrm{Ec} = 0.2$ (plate cooling), $\lambda = 1.0$, $\mathrm{Fs} = 0.055$, $\mathrm{Pr} = 1.0$ (geothermal fluids).

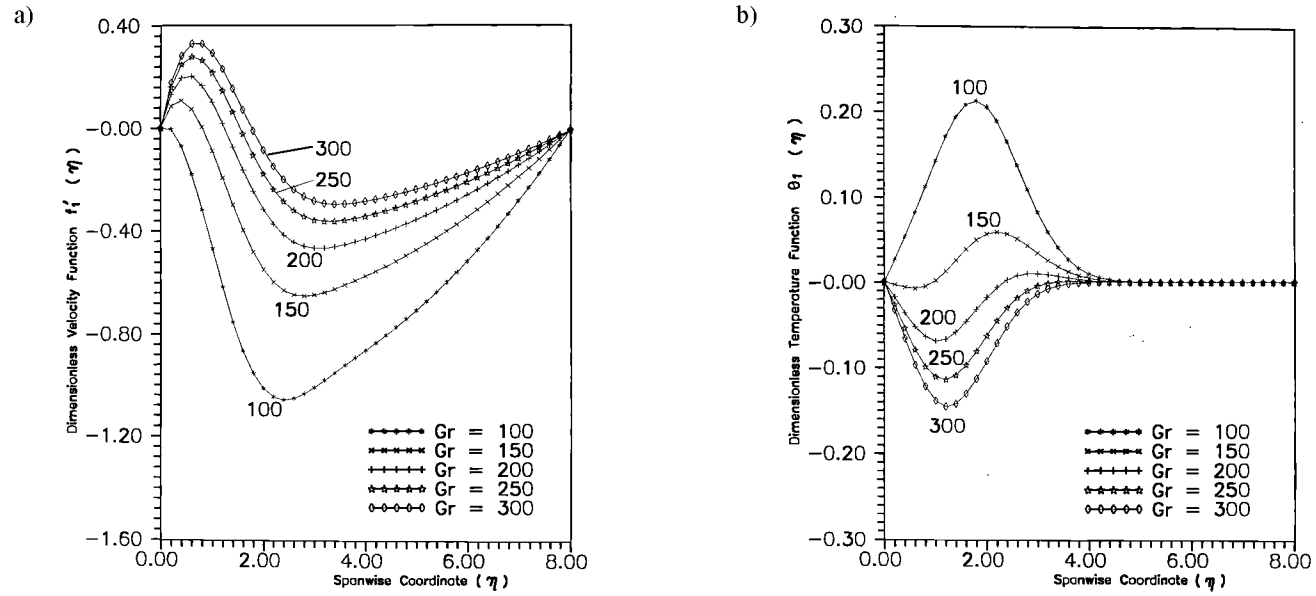

Fig. 7. Variation of $f_1'(\eta)$ and $\theta_1(\eta)$ with streamwise coordinate η. Results generated by DSRK scheme and Keller-Box for various Grashof numbers (GR): $\alpha = 1.0$, $\gamma = 0.1$, $\mathrm{Pr} = 1.0$, $\mathrm{Ec} = 0.2$, $\mathrm{Da} = 0.01$, $\mathrm{Ha} = 1.0$, $\mathrm{Fs} = 0.055$, $\lambda = 1.0$, $\mathrm{Re} = 1.0$.

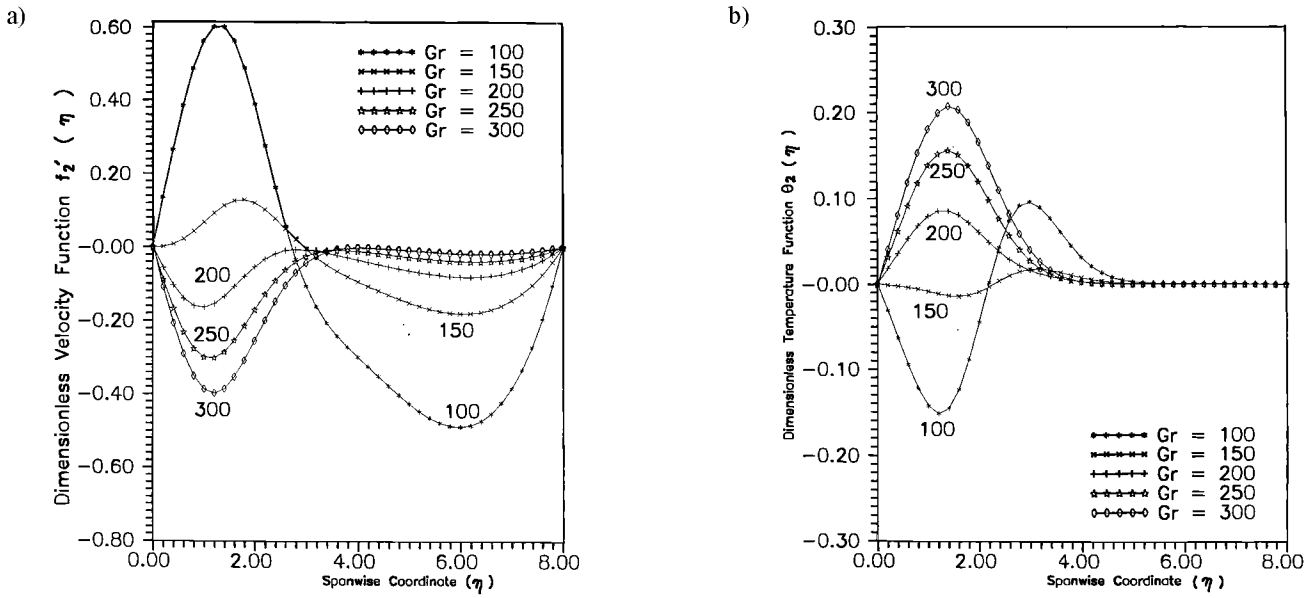

Fig. 8. Variation of $f_2'(\eta)$ and $\theta_2(\eta)$ with streamwise coordinate η. Results generated by DSRK scheme and Keller-Box for various Grashof numbers (GR) : $\alpha = 1.0$, $\gamma = 0.1$, $\mathrm{Pr} = 1.0$, $\mathrm{Ec} = 0.2$, $\mathrm{Da} = 0.01$, $\mathrm{Ha} = 1.0$, $\mathrm{Fs} = 0.055$, $\lambda = 1.0$, $\mathrm{Re} = 1.0$.

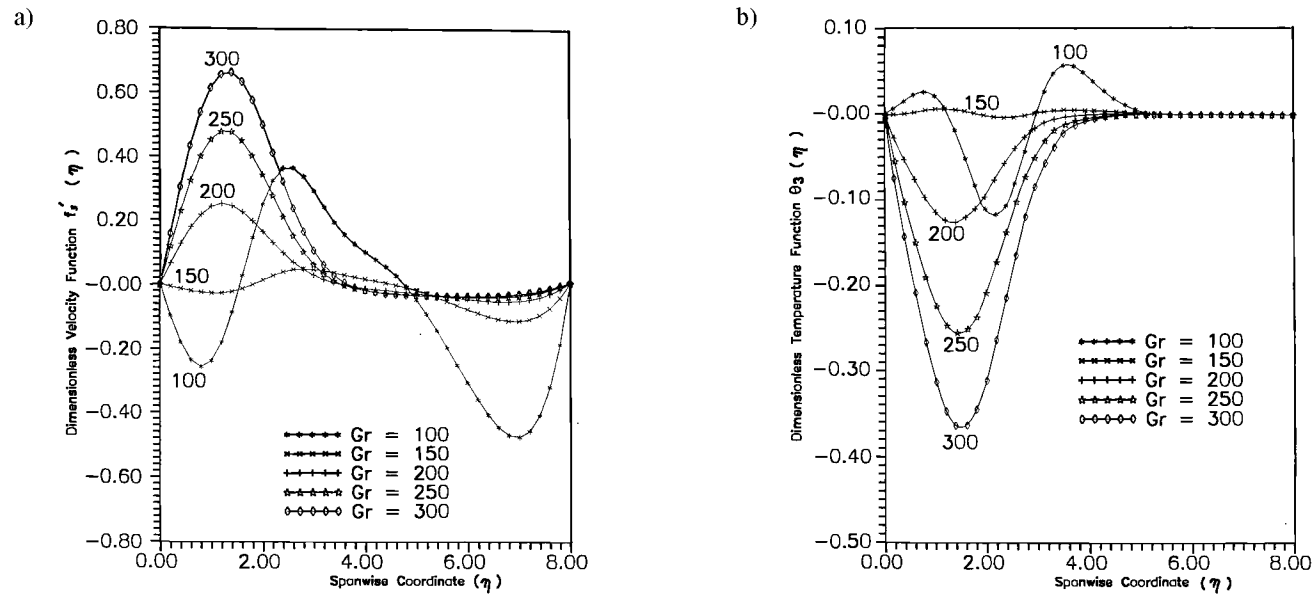

Fig. 9. Variation of $f_3'(\eta)$ and $\theta_3(\eta)$ with streamwise coordinate η. Results generated by DSRK scheme and Keller-Box for various Grashof numbers (GR): $\alpha = 1.0$, $\gamma = 0.1$, $\mathrm{Pr} = 1.0$, $\mathrm{Ec} = 0.2$, $\mathrm{Da} = 0.01$, $\mathrm{Ha} = 1.0$, $\mathrm{Fs} = 0.055$, $\lambda = 1.0$, $\mathrm{Re} = 1.0$.

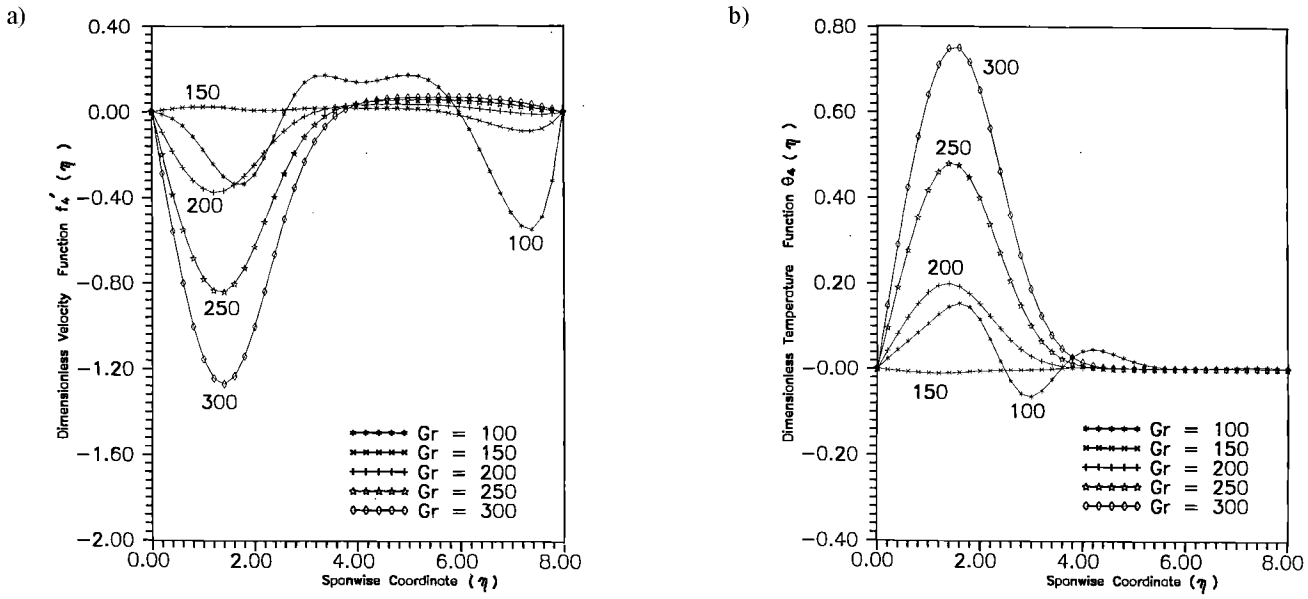

Fig. 10. Variation of $f_4'(\eta)$ and $\theta_4(\eta)$ with streamwise coordinate η. Results generated by DSRK scheme and Keller-Box for various Grashof numbers (GR): $\alpha = 1.0$, $\gamma = 0.1$, $\mathrm{Pr} = 1.0$, $\mathrm{Ec} = 0.2$, $\mathrm{Da} = 0.01$, $\mathrm{Ha} = 1.0$, $\mathrm{Fs} = 0.055$, $\lambda = 1.0$, $\mathrm{Re} = 1.0$.

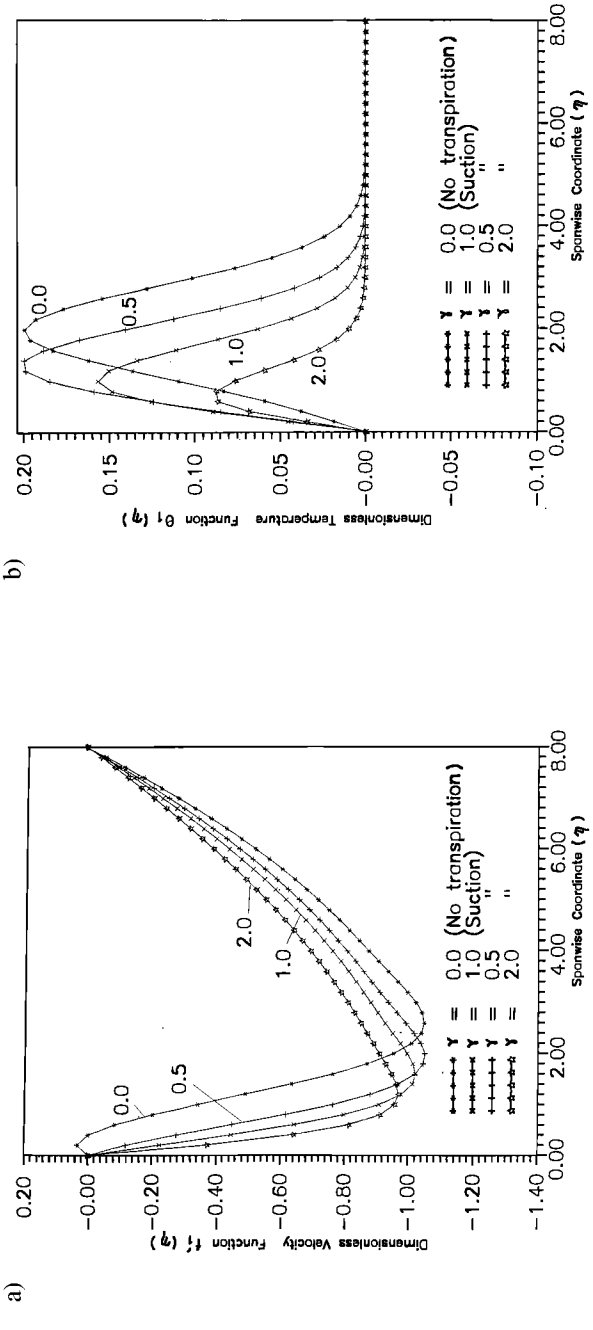

Fig. 11. Variation of $f_1'(\eta)$ and $\theta_1(\eta)$ with streamwise coordinate η. Results generated by DSRK scheme and Keller-Box for various transpiration parameters (γ): $\alpha = 1.0$, $\mathrm{Pr} = 1.0$, $\lambda = 1.0$, $\mathrm{Da} = 0.01$, $\mathrm{Gr} = 100$, $\mathrm{Ha} = 1.0$, $\mathrm{Fs} = 0.055$, $\mathrm{Re} = 1.0$, $\mathrm{Ec} = 0.1$.

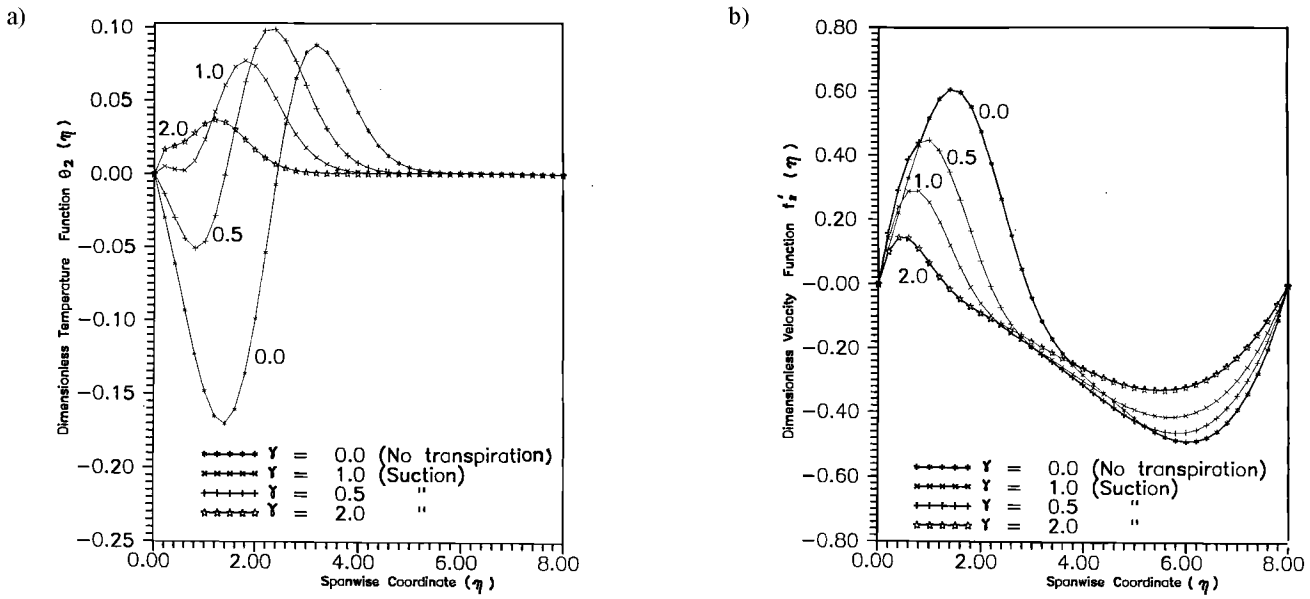

Fig. 12. Variation of $f_2'(\eta)$ and $\theta_2(\eta)$ with streamwise coordinate η. Results generated by DSRK scheme for various transpiration parameters (γ): $\alpha = 1.0$, $\mathrm{Pr} = 1.0$, $\lambda = 1.0$, $\mathrm{Da} = 0.01$, $\mathrm{Gr} = 100$, $\mathrm{Ha} = 1.0$, $\mathrm{Fs} = 0.055$, $\mathrm{Re} = 1.0$, $\mathrm{Ec} = 0.1$.

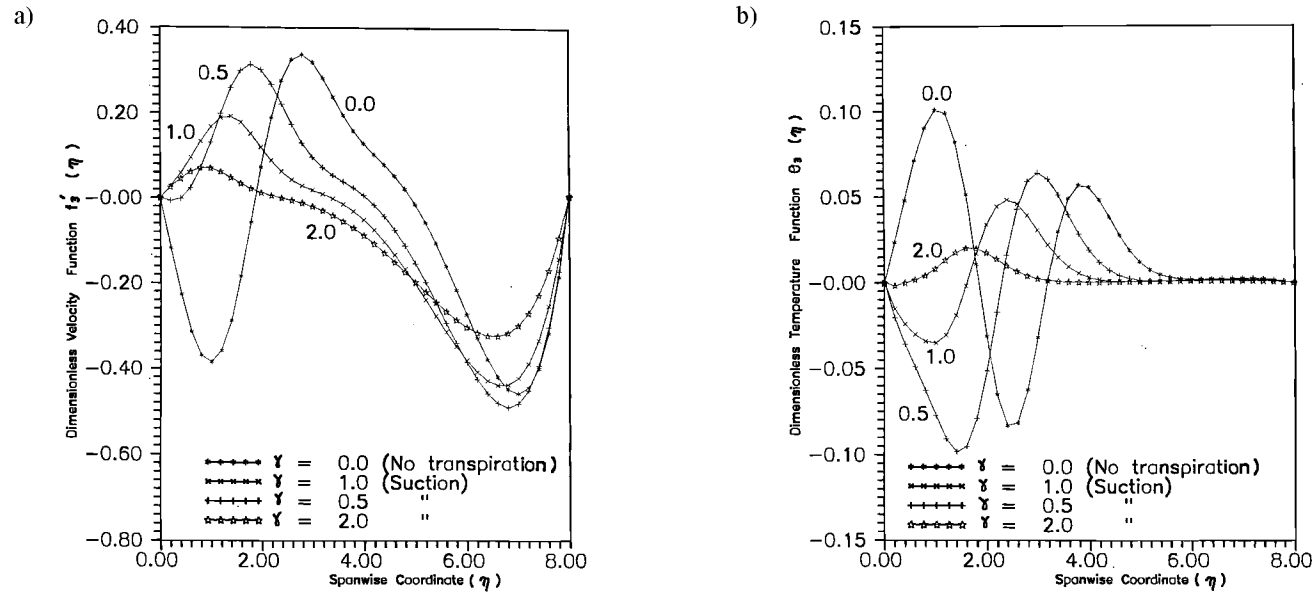

Fig. 13. Variation of $f_3'(\eta)$ and $\theta_3(\eta)$ with streamwise coordinate η. Results generated by DSRK scheme for various transpiration parameters (γ): $\alpha = 1.0$, $\mathrm{Pr} = 1.0$, $\lambda = 1.0$, $\mathrm{Da} = 0.01$, $\mathrm{Gr} = 100$, $\mathrm{Ha} = 1.0$, $\mathrm{Fs} = 0.055$, $\mathrm{Re} = 1.0$, $\mathrm{Ec} = 0.1$.

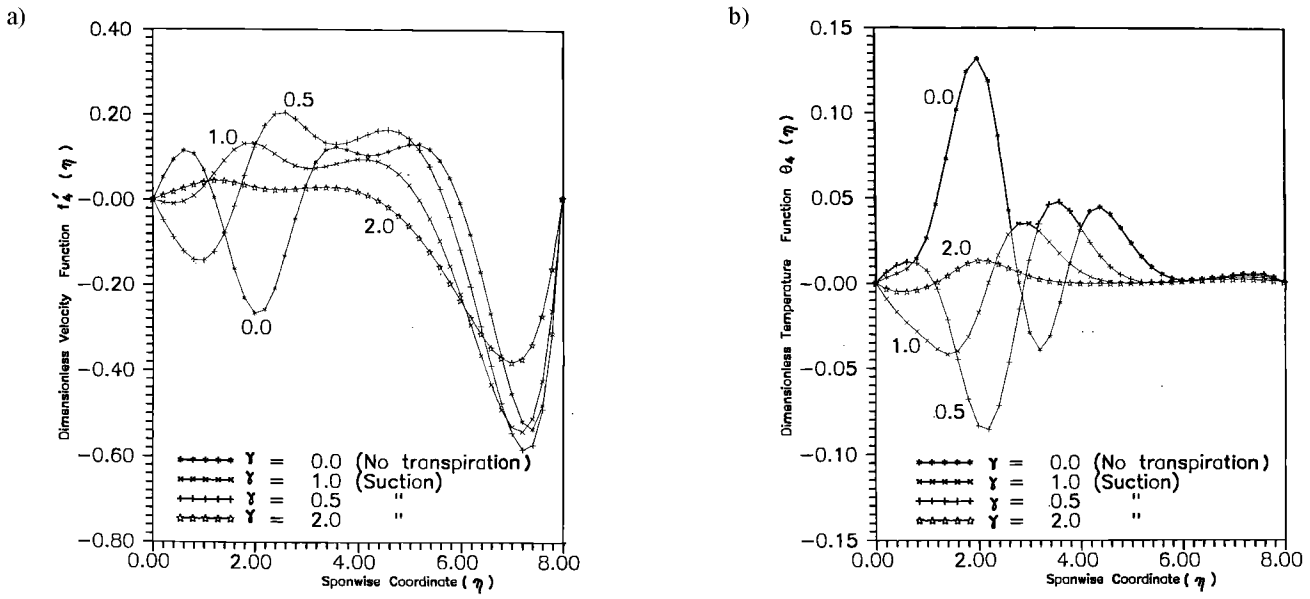

Fig. 14. Variation of $f_4'(\eta)$ and $\theta_4(\eta)$ with streamwise coordinate η. Results generated by DSRK scheme for various transpiration parameters (γ): $\alpha = 1.0$, $\mathrm{Pr} = 1.0$, $\lambda = 1.0$, $\mathrm{Da} = 0.01$, $\mathrm{Gr} = 100$, $\mathrm{Ha} = 1.0$, $\mathrm{Fs} = 0.055$, $\mathrm{Re} = 1.0$, $\mathrm{Ec} = 0.1$.

REFERENCES

1. Nield, D. A. and Bejan, A., *Convection in Porous Media*, Springer, New York, 1992.
2. Cheng, P. and Minkowycz, W. J., Free Convection about a Vertical Flat Plate Embedded in a Porous Medium With Application to Heat Transfer from a Dike, *J. Geophys. Resch*, 1981, **82**, pp. 2040–2044.
3. Vafia, K. and Tien, C. L., Boundary and Inertia Effects on Flow and Heat Transfer in Porous Media, *Int. J. Heat Mass Transfer*, 1981, **24**, pp. 195–203.
4. Lauriat, G. and Prasad, V., Non-Darcian Effects on Natural Convection in a Vertical Porous Enclosure, *Int. J. Heat Mass Transfer*, 1989, **32**, pp. 2135–2148.
5. Beckermann, C., Viskanta, R., and Ramadhyani, S., A Numerical Study of Non-Darcian Natural Convection in a Vertical Enclosure Filled with a Porous Medium, *Numer. Heat Transfer*, 1986, **10**, pp. 557–570.
6. Raptis, A. A. and Kafousias, N., Magnetohydrodynamic Free Convective Flow through a Torous Medium Bound by an Infinite Vertical Porous Plate with Constant Heat Flux, *Canad. J. Phys.*, 1982, **60**. No. 12, pp. 1725–1729.
7. Ram, P. C. and Takhar, H. S., Hall Effects on Oscillatory MHD Free Convective Flow through a Porous Medium, In: *Encyclopedia of Fluid Mechanics. Supplement 3, Advances in Flow Dynamics, chapter 12*, Chereminisoff, N. P., Ed., 1994, pp. 171–192.
8. Takhar, H. S. and Ram, P. C., Magnetohydrodynamic Free Convection Flow of Water at 4°C through a Porous Medium, *Int. Comm. Heat Mass Transfer*, 1994, **21**, pp. 371–376.
9. Takhar, H. S., Ram, P. C., Garba, E. J. D., and Bitok, J. K., Hydromagnetic Convective Flow of a Heat Generating Fluid past a Vertical Plate with Hall Currents and Constant Heat Flux through a Porous Medium, *J. Magnetohydrodynam. Plasma Resch*, 1995, **5**, pp. 185–195.
10. Gebhart B., Effects of Viscous Dissipation on Natural Convection, *J. Fluid Mech.*, 1962, **14**, pp. 225–232.
11. Nakayama, A. and Pop, I., Free Convection over a Non-Isothermal Body in a Porous Medium with Viscous Dissipation, *Int. Comm. Heat Mass Transfer*, 1989, **16**, pp. 173–180.
12. Takhar, H. S., Soundalgekar, V. M., and Gupta, A. S., Mixed Convection of an Incompressible Fluid in a Porous Medium past a Hot Vertical Plate, *Int. J. Non-Linear Mech.*, 1990, **25**, No. 6, pp. 723–728.
13. Takhar, H. S., Soundalgekar, V. M., and Beg, O. A., Darcy-Brinkman Thermal Boundary Layer Flow of an Incompressible Fluid through a Saturated Isotropic Homogeneous Porous Medium, *Int. J. Numerical Methods Engng*, 1995, **18**, pp. 559–589.
14. Cheng, P. and Chang, I., Buoyancy Induced Flows in a Saturated Porous Medium Adjacent to Impermeable Horizontal Surfaces, *Int. J. Heat Mass Transfer*, 1976, **19**, pp. 1267–1272.
15. Jang, J. Y. and Chang, W. J., Buoyancy-Induced Inclined Boundary-Layer Flow in a Saturated Porous Medium, *Comput. Methods. Appl. Mech.*, 1988, **68**, pp. 333–344.
16. Poulikakos, D., Buoyancy Driven Convection in a Horizontal Fluid Layer Extending over a Porous Substrate, *Phys. Fluids*, 1987, **29**, pp. 3949–3957.
17. Nakayama, A. and Koyama, H., Similarity Solutions for Buoyancy-Induced Flows over a Non-Isothermal Curved Surface in a Thermally Stratified Porous Medium, *Appl. Sci. Resch*, 1989, **46**, pp. 309–322.
18. Merkin, J. H., Free Convection Boundary Layers in a Saturated Porous Medium with Lateral Mass Flux, *Int. J. Heat Mass Transfer*, 1978, **21**, pp. 1499–1505.
19. Huang, M. J. and Chen, C. K., Effects of Surface Mass Transfer on Free Convection Flow over Vertical Cylinder Embedded in a Saturated Porous Medium, *ASME J. – Energy Resources Technology*, 1985, **107**, pp. 394–396.

20. Ramaniah, G. and Malarvizhi, G., Non-Darcy Regime Mixed Convection on Vertical Plates in Saturated Porous Media with Lateral Mass Flux, *Acta Mechanica*, 1990, **81**, pp. 191–200.
21. Cebeci, T. and Bradshaw, P., *Physical and Computational Aspects of Convective Heat Transfer*, Springer-Verlag, Berlin, 1984.
22. Keller, H. B., Numerical Methods in boundary Layer Theory, *Ann. Review Fluid Mech.*, 1978, **10**, pp. 417–433.
23. Keller, H. B., Accurate Difference Methods for Two-Point Boundary Value Problems, *SIAM J. Numer. Analysis*, 1974, **11**, pp. 305–320.
24. Cebeci, T. and Smith, A. M. O. *Analysis of Turbulent Boundary Layers*, Applied Mathematics and Mechanics: Monographs, 1974.
25. Ingham, D. B. and Pop, I., Mixed Convection about a Cylinder Embedded to a Wedge in Porous Media, *AIAA J. Thermophys.*, 1991, **5**, No. 1, pp. 117–120.
26. Hossain M. A., Effect of Transpiration on Combined Heat and Mass Transfer in Mixed Convection along a Vertical Plate, *Int. J. Energy Resch*, 1992, **16**, pp. 761–769.
27. Gorla, R. S. R. and Pop, I., Conjugate Heat Transfer with Radiation from a Vertical Circular Pin in a Non-Newtonian Ambient Medium, *Warme-und-Stofrubertragung*, 1993, **28**, No. 11.
28. Gorla, R. S. R. and Takhar, H. S., Combined Convective Heat Transfer from a Flat Plate Embedded in Porous Media, *Int. J. Eng. Fluid Mech.*, 1991, **4**, pp. 363–373.
29. Gebhart, B., Jaluria, Y., Roop, L. M., and Sammakia, B., *Buoyancy-Induced Flows and Transport*, Hemisphere Publishing Corporation, New York, 1988.
30. Chandrasekhar, S., *Hydrodynamic and Hydromagnetic Stability*, Oxford University Press, Clarendon, 1961.
31. Prasad, V. and Kladias, N., Non-Darcy Natural Convection in Saturated Porous Media, In: *Convective Heat and Mass Transfer in Porous Media, Kakac, S. et al., Eds.*, Kluwer Academic, Dordrecht, 1991, pp. 173–224.

□◆◆◆□